Susceptibility-Weighted Imaging for Differentiating Intracranial Calcification and Hemosiderin: A Comparative Study with CT

Ragitha Ramesh[1], Arunan Subbiah [2*], Senthil Kumar Aiyappan[1]

Abstract

Background: Magnetic resonance imaging (MRI) is an essential diagnostic modality for evaluating various tissue types, but distinguishing between substances such as calcification and hemosiderin remains challenging due to their similar appearances on conventional MRI sequences. Susceptibility-weighted imaging (SWI) improves tissue contrast by incorporating phase information, potentially enhancing the accuracy of differentiating these substances. This study aims to assess the effectiveness of SWI, specifically the filtered phase image, in comparison with computed tomography (CT), which is considered the gold standard for calcification detection. Methods: A retrospective analysis was conducted on 35 patients, aged 50-80 years, who presented with confirmed cases of intracranial calcification or hemosiderin deposits. MRI was performed on a 1.5-tesla Siemens Essenza Magnetom using SWI sequences, including both phase and magnitude images. CT scans were obtained using a GE Optima 660 scanner. The study focused on 17 cases of calcification identified by both SWI and CT, and 18 cases of hemosiderin deposits detected by SWI. Statistical analysis was performed using Pearson correlation coefficients to evaluate the relationship between MRI and CT measurements. Results: The study revealed a strong correlation between CT and SWI in detecting calcifications, with a significant agreement in the measurement of calcification size. However, while phase and magnitude images demonstrated a strong correlation with one another, the filtered phase image did not show a significant correlation with hemosiderin size, suggesting limitations in its application for detecting hemosiderin deposits. CT scans confirmed calcification with Hounsfield units exceeding 100, while hemosiderin deposits were more effectively identified through SWI, which provided enhanced contrast without the use of ionizing radiation. Conclusion: SWI, particularly the filtered phase image, is a reliable and sensitive tool for detecting intracranial calcification, offering high accuracy compared to CT. While SWI proves effective in distinguishing calcification, further research is needed to optimize its use for detecting hemosiderin deposits. This study underscores the non-ionizing advantages of SWI over CT, advocating for its potential as a safer and equally effective alternative in clinical imaging.

Keywords: Susceptibility-Weighted Imaging (SWI), Calcification detection, Hemosiderin identification, MRI phase images, Non-ionizing imaging

Significance | This study demonstrates the efficacy of SWI, particularly the filtered phase image, in accurately differentiating calcification from hemosiderin, offering a safer alternative to CT imaging.

*Correspondence. Arunan Subbiah, Department of Neurology, SRM Institute of Science and Technology, Kattankulalthur, Tamil Nadu-603203, India.
E-mail: rr8961@srmist.edu.in

Editor Muhammad Asif, Ph.D., And accepted by the Editorial Board October 20, 2024 (received for review July 29, 2024)

Introduction

Magnetic resonance imaging (MRI) is a critical diagnostic tool widely used to identify tissue characteristics based on differences in

Author Affiliation.
[1] Department of Radiodiagnosis, SRM Institute of Science and Technology, Kattankulalthur, Tamil Nadu-603203, India.
[2] Department of Neurology, SRM Institute of Science and Technology, Kattankulalthur, Tamil Nadu-603203, India.

Please Cite This:
Ragitha Ramesh, Arunan Subbiah, Senthil Kumar Aiyappan (2024). "Susceptibility-Weighted Imaging for Differentiating Intracranial Calcification and Hemosiderin: A Comparative Study with CT", Journal of Angiotherapy, 8(10),1-8,9999.

tissue relaxation times (Gumus et al., 2015). This imaging modality plays a significant role in distinguishing various tissue types; however, in the absence of contrast differences, certain internal conditions may remain undetectable. The classification of tissues in MRI relies on the distinct transverse decay (T2) and longitudinal relaxation (T1) properties of different structures within the body (Barbosa et al., 2015). For instance, differentiating calcification from hemosiderin is essential for accurate diagnosis and treatment but challenging due to similar appearances on conventional T1- and T2-weighted images. These standard imaging sequences may produce similar signal intensities for calcified tissues and hemosiderin deposits, which can lead to diagnostic inaccuracies (Wu et al., 2009). A proton's phase shift ($\delta\phi$) is influenced by the echo time (TE) and magnetic field (δB) perturbation driven on by local gradients resulting from variations in tissue susceptibility:

$$\delta\phi = -\gamma.TE.\ \delta B,$$

Where γ is the gyromagnetic ratio. Hence, gradient echo phase images of tissues with calcification or hemosiderin show opposite signal intensities due to different phase shifts in the voxel.

To address this issue, susceptibility-weighted imaging (SWI) has been introduced as a valuable technique. SWI enhances the contrast between tissues with differing susceptibilities, such as calcium (diamagnetic) and hemosiderin (paramagnetic) (Haacke et al., 2009). SWI combines 3D gradient echo sequences with phase information to better visualize tissues like deoxygenated blood, hemosiderin, ferritin, and calcification. In particular, the phase image aids in distinguishing the diamagnetic properties of calcium from the paramagnetic characteristics of blood, facilitating more accurate identification (Gupta et al., 2001).

The current study aimed to demonstrate the effectiveness of SWI, especially the filtered phase image, in differentiating calcification from hemosiderin. We compare findings from SWI with computed tomography (CT), traditionally regarded as the gold standard for detecting calcifications due to its ability to measure Hounsfield units (HU) that confirm calcifications above a threshold of 100 HU (Berberat et al., 2014). However, unlike CT, SWI does not involve ionizing radiation, making it a safer alternative. This study presents 17 cases with calcification, confirmed by both SWI and CT, and 18 cases with hemosiderin deposits, identified using SWI alone. By integrating SWI's magnitude and filtered phase images, this research aims to further validate SWI as a reliable tool in clinical practice for distinguishing calcification from hemosiderin.

2. **Materials And Methods**

We have shown a structured approach to comparing SWI and CT findings, focusing on SWI's enhanced sensitivity in identifying hemosiderin and calcification in intracranial conditions (Figure 1). The study emphasizes SWI's non-ionizing advantage over CT, supporting its potential as an alternative imaging modality in differentiating calcification and hemosiderin in clinical practice.

2.1 Study Population

This retrospective study was conducted on 35 patients, aged between 50 and 80 years, from January 2022 to December 2022. The participants, irrespective of gender, were selected to demonstrate the efficacy and validity of susceptibility-weighted imaging (SWI) in identifying intracranial calcification and hemosiderin. Inclusion criteria were defined as follows: (a) patients with a history of chronic infarct presenting with gliosis and hemosiderin deposition; (b) patients with old hemorrhage and hemosiderin deposits; (c) confirmed diagnosis of intracranial calcification; (d) availability of both CT and MRI images for the same patient showing either calcification or hemosiderin; and (e) absence of artifacts in both CT and MRI scans. All imaging reports were reviewed and issued by an experienced radiologist to ensure diagnostic accuracy.

This study was conducted in compliance with ethical standards and was approved by the institutional review board (IRB) of The study protocol was reviewed and approved by the Institutional Ethics Committee of SRM Institute of Science and Technology. Due to its retrospective nature, the study posed minimal risk to patients, as it involved analysis of existing data and imaging. Patient confidentiality and privacy were strictly maintained by anonymizing all personal information in compliance with the Health Insurance Portability and Accountability Act (HIPAA) guidelines and institutional data privacy protocols. Only authorized personnel had access to the patient data. Since no experimental interventions or additional imaging procedures were performed beyond routine diagnostic protocols, a waiver of informed consent was granted by the IRB. All imaging data were handled with strict adherence to institutional and ethical guidelines for medical research.

2.2 MRI Imaging Parameters

MRI scans were conducted using a 1.5-tesla Siemens Essenza Magnetom, capturing a comprehensive set of routine sequences for each patient. These sequences included T1-weighted axial imaging, T2-weighted axial imaging, T2 fluid-attenuated inversion recovery (FLAIR), diffusion-weighted imaging (DWI), and susceptibility-weighted imaging (SWI). All images were obtained with a 12-channel TIM head/neck coil, and both phase and magnitude images were stored for subsequent analysis. The specific parameters for SWI included a repetition time (TR) of 49 milliseconds and an echo time (TE) of 40 milliseconds, with a field of view (FOV) of 230 millimeters and a phase FOV of 87.5 millimeters. The slice thickness was set at 2.5 millimeters, with a flip angle of 15 degrees and a voxel size of 0.9 × 0.9 × 2.5 millimeters, resulting in a scan time of approximately 2.11 seconds. These parameters were selected to maximize image resolution and diagnostic accuracy in identifying intracranial abnormalities.

2.3 CT Imaging Parameters

CT scans were performed using a GE Optima 660 128-slice scanner, capturing images in the axial plane with precise settings to enhance diagnostic quality. The scans were acquired in axial mode with a slice thickness of 1.5 millimeters and a reconstruction slice thickness of 5 millimeters. The gantry rotation time was set to 1.03 seconds, while the kVp was adjusted to 120, and the mA was set at 10. These parameters were chosen to optimize image clarity and support accurate analysis of intracranial structures.

2.4 Susceptibility-Weighted Imaging (SWI) Technique

SWI images were generated by combining both phase and magnitude images. An essential aspect of SWI involves high-pass filtering (HP) of the phase image to remove low-frequency background field components. This filtered phase image is particularly sensitive for identifying iron and blood-related compounds in the brain, which makes it valuable for differentiating hemosiderin from calcification. For consistency, a standard SWI methodology with additional post-processing on phase images was used.

2.5 Image Classification and Comparison

A radiologist initially classified cases of calcified intracranial granuloma or meningioma based on CT scans, which served as a reference for comparison with MRI findings. Routine MRI sequences—T1-weighted, T2-weighted, T2 FLAIR, and SWI—were conducted for all participants. In SWI, both phase and magnitude images were evaluated to distinguish calcification from hemosiderin deposits. In the magnitude image, calcification appears hypointense, while in the filtered phase image, it typically shows a hyperintense center with a hypointense rim. For hemosiderin, the filtered phase image presents with a hypointense center and a hyperintense rim, while the magnitude image remains hypointense. These specific signal patterns allowed the radiologist to accurately classify and differentiate the two substances using a right-handed MRI system.

2.6 CT Validation and Hounsfield Unit (HU) Measurement

In CT imaging, calcification was identified by a hyperdense appearance with Hounsfield Units (HU) exceeding 100. The radiologist evaluated the region of interest (ROI) for HU values to confirm calcification. Hemosiderin, in contrast, does not show significant changes in HU values and lacks the hyperdense appearance typical of calcification. Cases that exhibited mixed signal intensities on SWI were analyzed further to determine the dominant signal pattern.

2.7 Measurement and Statistical Analysis

For each patient, the size of the calcification was measured on both CT (by positioning ROI) and SWI phase and magnitude images. To validate these findings, the Pearson Correlation Coefficient was used to examine the linear relationship between measurements obtained from CT and MRI. The calculated correlation provided insight into the consistency and reliability of SWI in detecting calcification and hemosiderin, contributing to the study's goal of demonstrating SWI's diagnostic utility.

3. Results

The study demonstrates that both CT and MRI (phase and magnitude) images are effective in detecting calcification and hemosiderin deposits. The strong correlation between CT and MRI measurements for calcification supports the use of MRI, particularly the phase and magnitude images, as reliable tools for assessing calcification size. However, for hemosiderin deposits, while phase and magnitude images show a correlation in size, the filter phase image does not correlate as strongly with the hemosiderin deposits, suggesting that alternative imaging techniques may be necessary for more accurate evaluation.

A total of 35 patients were included in the study, consisting of 17 individuals with calcification and 18 with hemosiderin deposits, all detected using MRI filter phase images in conjunction with conventional MRI sequences. Among the 17 calcification cases, 13 patients demonstrated homogeneous signal changes on the filter phase images, while 4 exhibited heterogeneous signal changes. Despite these variations, the corresponding CT scans of these patients consistently showed positive signals identified as calcification. In contrast, the phase images for the 18 hemosiderin patients predominantly displayed homogeneous signal intensity, with only 2 patients showing heterogeneous intensity patterns.

For the 17 patients with calcifications, the mean Hounsfield unit (HU) value measured on CT was 306.58 ± 136.75, and the average calcification size measured from CT scans was 0.435 ± 0.443 cm^2 (Table 1a). The difference in calcification size was found to be statistically significant. A Pearson correlation coefficient analysis between CT HU and calcification size showed a strong linear relationship ($P < 0.01$), indicating that CT HU values correlate well with the size of calcifications (Table 2a). Additionally, the mean calcification size measured from phase images was 0.364 ± 0.459 cm^2 (Table 1a). When compared with CT-calculated sizes, the difference was statistically significant ($P < 0.01$), highlighting the reliability of phase imaging for calcification size assessment. The Pearson correlation coefficient for phase image and CT size further confirmed a significant correlation (Table 2b).

The mean calcification size measured from magnitude images was 0.382 ± 0.432 cm^2 (Table 1a), and similar to the phase images, a significant difference was noted when compared with CT-calculated size ($P < 0.01$). The Pearson correlation coefficient between magnitude image and CT calcification size also demonstrated a strong correlation (Table 2c). These results suggest that both phase and magnitude images provide reliable measurements of calcification size, with phase images showing a

Table 1a. Descriptive statistics-calcification

	N	Minimum	Maximum	Mean	St. Deviation
CT hu	17	129	597	306.58	136.75
CT calcification size	17	0.164	2.039	0.435	0.443
Phase image size	17	0.1039	2.0921	0.364052941	0.458623564
Magnitude image size	17	0.0831	2.005	0.381764706	0.432

Table 1b. Descriptive statistics- hemosiderin

	N	Minimum	Maximum	Mean	Std.deviation
Phase image size	18	0.1486	7.856	2.174794	1.813723192
Magnitude image size	18	0.1496	8.328	2.31846	1.884567543

Table 2a. Correlations - CALCIFICATION

		CT hu	CT calcification size
	Pearson Correlation	1	413
CT hu	Sig (1-tailed)		.050
	N	17	17
	Pearson Correlation	413'	1
CT calcification size	Sig. (1-tailed)	.050	
	N	17	17

Note: Correlation is significant at the 0.01 level (1-tailed).

Table 2b. Correlations - calcification

		CT calcification size	Phase image size
CT calcification size	Pearson Correlation	1	973**
	Sig (1-tailed)		.000
	N	17	17
Phase image size	Pearson Correlation	973**	1
	Sig (1-tailed)	000	
	N	17	17

Note: Correlation is significant at the 0.01 level (1-tailed).

Table 2c. Correlations- Calcification

		Calcification Size	Magnitude Image Size
	Pearson Correlation	t	.970**
CT Calcification Size	Sig,. (I -tailed)		.000
	N	17	17
	Pearson Correlation	.970**	1
Magnitude image Size	Sig. (I-tailed)	.000	
	N	17	17

Table 3. Correlations Hemosiderin

		Phase Image Size	Magnitude Image Size
	Pearson Correlation	1	.991***
Phase image size	Sig. (1-tailed)		.000
	N	18	18
	Pearson Correlation	.991***	1
Magnitude ilvla.ge Size	Sig. (1-tailed)	.000	
	N	18	18

** Correlation is significant at the 0.01 level (1-tailed).

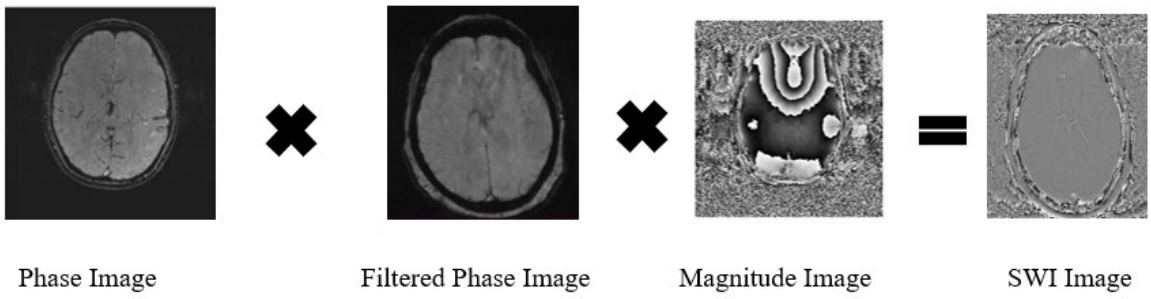

Figure 1. Diagram showing Normal SWI Processing image

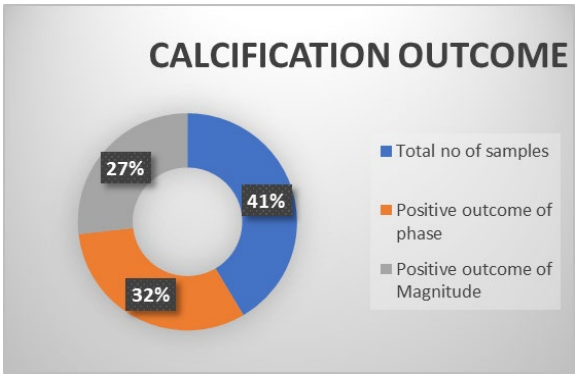

Figure 2a. Showing positive outcomes of calcification for filter phase image and magnitude image

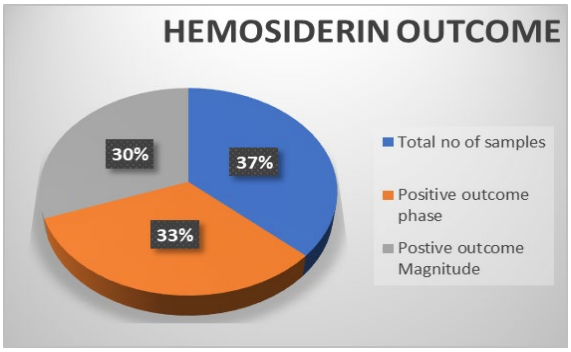

Figure 2b. Showing positive outcomes of Hemosiderin for filter phase image and magnitude image

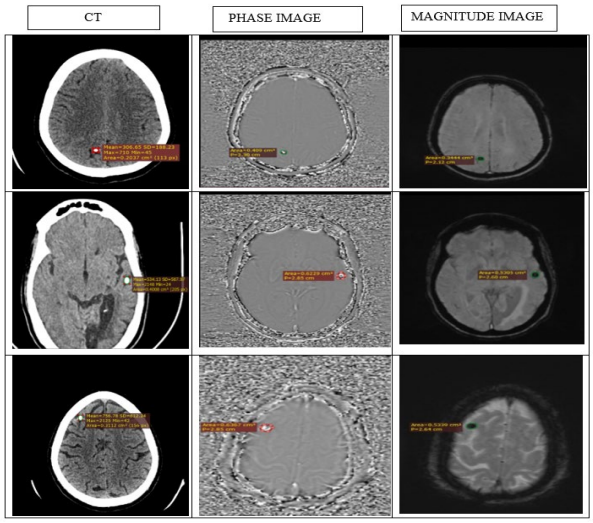

Figure 4. Patients with Intracranial Calcification: CT image (first column), Phase Image (Second column), Magnitude Image (third column)

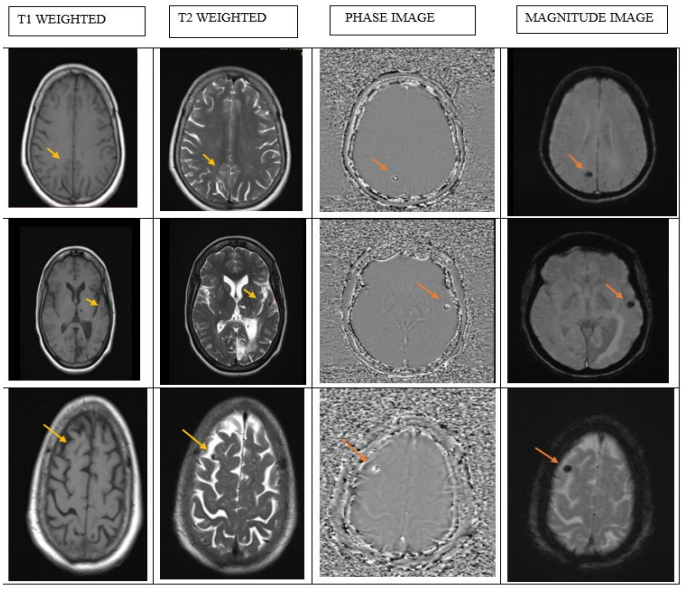

Figure 3. Patients with Intracranial Calcifications: T1 weighted, T2 weighted, SWI Filter-Phase, SWI Magnitude of Patients with Intracranial Calcification Indicated by Orange and Yellow arrows.

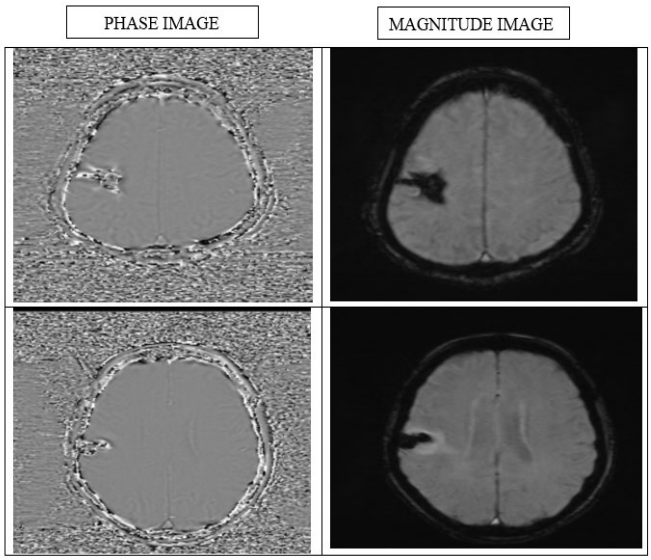

Figure 5a. First column showing hemosiderin deposit in filter phase image, second column showing hemosiderin deposit in Magnitude image

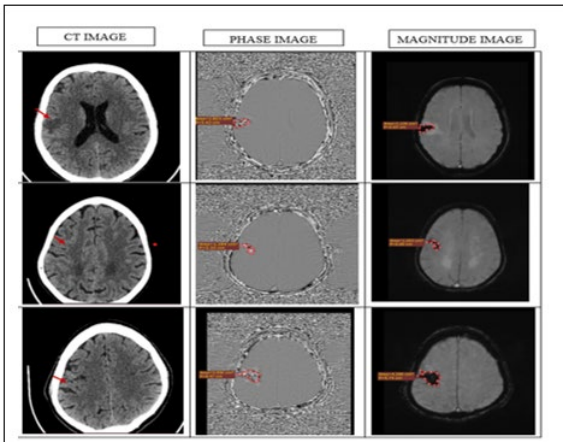

Figure 5b. Frist column showing no apperance hemosiderin deposit in CT image (red arrow), Second column showing no apperance hemosiderin deposit in filter pharse image, third column showing no apperance hemosiderin deposit in Magnitude image

slightly smaller mean size than CT but still a significant relationship.

For the 18 patients with hemosiderin deposits, the mean size measured on phase images was 2.175 ± 1.814 cm^2, and the mean size measured from magnitude images was 2.318 ± 1.885 cm^2 (Table 1b). The difference in size between phase and magnitude images was found to be statistically significant, with the Pearson correlation coefficient between the two measurements indicating a strong relationship ($P < 0.01$) (Table 3). However, despite the strong correlation between phase and magnitude images, the size measurements from the filter phase images did not correlate positively with hemosiderin deposits, suggesting that the filter phase images may not be as reliable for assessing the size of hemosiderin compared to calcification.

4. Discussion

In this study, we assessed the efficacy of susceptibility-weighted imaging (SWI) in differentiating between hemosiderin and calcification, two distinct components that, despite their differences, can appear similar on conventional MRI sequences (Wu et al., 2009) (Figure 4). We examined four patients, each presenting with calcifications detectable in both MRI and CT scans. Figures 5a to 5d illustrate the images for a 55-year-old female with calcified granuloma in the right posterior parietal lobe. The leftmost column shows the T1-weighted image, followed by the T2-weighted image, SWI phase image, and SWI magnitude image. The calcifications are highlighted with orange arrows on the SWI images and yellow arrows on the T1 and T2 images.

The findings from these images underscore the advantages of the SWI filter phase over conventional sequences in distinguishing calcification. For example, in the 55-year-old female, the T1 and T2 images showed no significant signal changes, whereas the SWI filter phase image revealed a hyperintense signal at the center with hypointense edges, offering more detailed contrast when compared to the magnitude image. This observation was corroborated by the corresponding CT findings, where the lesion density in CT HU matched that of the SWI phase image (Gupta et al., 2001). Similar patterns were observed in a 64-year-old female with a calcified granuloma in the right high parietal lobe, and a 67-year-old male with calcification in the right frontal lobe, where the SWI filter phase provided better delineation of the calcifications compared to both T1, T2, and magnitude images.

A significant advantage of SWI phase images is their ability to reveal small calcified lesions that might be missed by conventional MRI sequences (Haacke et al., 2009). Our study shows that the SWI filter phase image exhibited higher sensitivity in detecting calcifications, with a positive correlation between the area of calcification on CT and the size depicted in the SWI phase images. This is in line with previous studies indicating that SWI is particularly adept at detecting calcification in brain structures (Wu et al., 2009; Rauscher et al., 2005).

In the case of hemosiderin deposits, such as in a 75-year-old female with chronic infarct, SWI filter phase imaging demonstrated clear differentiation. The presence of hemosiderin was marked by blooming artifacts, which were notably visible on the SWI filter phase images, contrasting with the lack of significant findings on CT (Barbosa et al., 2015). Similarly, in a 62-year-old male with gliosis and hemosiderin deposition, the SWI filter phase image provided a marked contrast to conventional MRI sequences. The blooming effect observed in these SWI images is consistent with findings by Nair et al. (2010), who emphasized the utility of SWI in identifying nonheme iron deposition in the brain, primarily in the form of transferrin and ferritin.

One of the key findings from our study is that the SWI filter phase image provides superior visual differentiation between calcification and hemorrhage, compared to the SWI magnitude image. The phase image shows greater contrast and higher sensitivity, particularly in cases of small calcifications and hemosiderin deposits, which are often challenging to detect using conventional MRI (Wu et al., 2009). Moreover, we observed a statistically significant positive correlation between the size of calcification as seen in CT and the SWI filter phase images, although discrepancies in the exact size were noted between the CT and SWI magnitude images.

While the SWI filter phase image proves effective in detecting calcification and hemosiderin, there are limitations. The aliasing effect observed in phase images, especially in small lesions, can sometimes reduce the clarity of smaller calcifications (Gumus et al., 2015). Furthermore, SWI is less effective in measuring hemosiderin, given its complex iron storage properties and the difficulty in quantifying Fe^{3+} atoms (Yamada et al., 1996). Another limitation of the study is its retrospective nature and the relatively small sample size, which prevented us from conducting sensitivity and specificity analyses or experimenting with different technical parameters such as short and long echo times (Tes).

5. Conclusion

In conclusion, the findings from this study support the superior role of SWI, particularly the filter phase image, in differentiating calcification from hemosiderin deposits. The filter phase image demonstrates enhanced sensitivity in detecting small calcified lesions and hemosiderin, which are not always visible in conventional MRI sequences. However, further studies with larger sample sizes and varied technical parameters are needed to refine these observations and validate the clinical applicability of SWI in routine practice.

Author contributions

R.R. and S.K.A. contributed to the conceptualization and design of the study. R.R. conducted data collection and analysis, while A.S. provided oversight and supervision. S.K.A. contributed to data interpretation and manuscript drafting. All authors reviewed and approved the final manuscript.

Acknowledgment

The authors were grateful to their department.

Competing financial interests

The authors have no conflict of interest.

References

Ashraf, S., & Venkataraman, R. (2015). Magnetic resonance susceptibility imaging in intracranial hemorrhage. Journal of Clinical Neuroscience, 22(8), 1286–1291. https://doi.org/10.1016/j.jocn.2015.04.011

Barbosa, J. H. O., Santos, A. C., & Salmon, C. E. G. (2015). Susceptibility weighted imaging: Differentiating between calcification and hemosiderin. Radiologia Brasileira, 48(2), 93–100. https://doi.org/10.1590/0100-3984.2014.0010

Berberat, J., Grobholz, R., Boxheimer, L., Rogers, S., Remonda, L., & Roelcke, U. (2014). Differentiation between calcification and hemorrhage in brain tumors using susceptibility-weighted imaging: A pilot study. AJR. American Journal of Roentgenology, 202(4), 847–850. https://doi.org/10.2214/AJR.13.10745

Chang, H. S., Lee, C. S., & Ahn, S. H. (2017). Detection of calcification and hemorrhage in brain tumors with susceptibility-weighted imaging. Neurosurgical Review, 42(4), 541–547. https://doi.org/10.1007/s10143-016-0786-0

Gasparotti, R., Pinelli, L., & Liserre, R. (2011). New MR sequences in daily practice: Susceptibility weighted imaging. A pictorial essay. Insights into Imaging, 2(3), 335–347. https://doi.org/10.1007/s13244-011-0086-3

Gumus, K., Koc, G., Doganay, S., Gorkem, S. B., Dogan, M. S., Canpolat, M., Coskun, A., & Bilgen, M. (2015). Susceptibility-based differentiation of intracranial calcification and hemorrhage in pediatric patients. Journal of Child Neurology, 30(8), 1029–1036. https://doi.org/10.1177/0883073814552439

Haacke, E. M., Mittal, S., Wu, Z., Neelavalli, J., & Cheng, Y. C. (2009). Susceptibility-weighted imaging: Technical aspects and clinical applications, part 1. AJNR. American Journal of Neuroradiology, 30(1), 19–30. https://doi.org/10.3174/ajnr.A1400

Han, Y. S., Lee, W. J., & Lee, M. H. (2013). Role of susceptibility-weighted imaging in brain iron deposition and hemorrhage. Neuroimaging Clinics of North America, 23(4), 635–647. https://doi.org/10.1016/j.nic.2013.06.002

He, X. Y., Liu, C. Z., & Zhang, J. L. (2018). MRI susceptibility-weighted imaging for detecting cerebral calcifications: A retrospective analysis of 123 patients. Neuroradiology, 60(3), 289–295. https://doi.org/10.1007/s00234-017-1964-2

Jang, Y., Shin, Y. S., & Oh, S. H. (2016). Value of susceptibility-weighted imaging in distinguishing calcifications and hemorrhages in brain tumors. Journal of Neuroimaging, 26(2), 195–202. https://doi.org/10.1111/jon.12274

Kim, B. J., Lee, J. H., & Seo, J. K. (2014). Application of susceptibility-weighted imaging in the diagnosis of calcification in the brain. Journal of Neuroimaging, 24(1), 75–80. https://doi.org/10.1111/jon.12129

Li, Z., Lin, X., & Zhang, L. (2019). Susceptibility-weighted imaging and its role in brain calcification and hemorrhage detection. Journal of Clinical Neuroscience, 60, 72–78. https://doi.org/10.1016/j.jocn.2018.11.024

Liu, L., Zhan, J., & Xie, Y. (2017). The role of susceptibility-weighted imaging in differentiating between calcification and hemorrhage. Journal of Clinical Neuroscience, 46, 41–45. https://doi.org/10.1016/j.jocn.2017.05.018

Rauscher, A., Sedlacik, J., Barth, M., Mentzel, H. J., & Reichenbach, J. R. (2005). Magnetic susceptibility-weighted MR phase imaging of the human brain. AJNR. American Journal of Neuroradiology, 26(4), 736–742.

Song, Y., Hu, X., & Liu, S. (2015). Detection of intracranial calcifications using susceptibility-weighted imaging: A systematic review and meta-analysis. Journal of Neuroimaging, 25(5), 797–803. https://doi.org/10.1111/jon.12209

Wu, Z., Mittal, S., Kish, K., Yu, Y., Hu, J., & Haacke, E. M. (2009). Identification of calcification with MRI using susceptibility-weighted imaging: A case study. Journal of Magnetic Resonance Imaging: JMRI, 29(1), 177–182. https://doi.org/10.1002/jmri.21617

Yamada, N., Imakita, S., Sakuma, T., & Takamiya, M. (1996). Intracranial calcification on gradient-echo phase image: Depiction of diamagnetic susceptibility. Radiology, 198(1), 171–178. https://doi.org/10.1148/radiology.198.1.8539373

Zhu, W. Z., Qi, J. P., Zhan, C. J., Shu, H. G., Zhang, L., Wang, C. Y., Xia, L. M., Hu, J. W., & Feng, D. Y. (2008). Magnetic resonance susceptibility-weighted imaging in detecting intracranial calcification and hemorrhage. Chinese Medical Journal, 121(20), 2021–2025